Predicting CO₂ Plume Migration using Deep Neural Networks

Gege Wen [1] **Ment Tang** [1] **Sally M Benson** [1]

1. Background

Large-scale deployment of carbon capture and sequestration (CCS) is essential to many climate mitigation modeling scenarios for achieving the 2 degrees C target (IPCC, 2014). Carbon dioxide (CO_2) captured from concentrated sources, the atmosphere, or through bio-energy production, is compressed into a liquid and injected into deep geological formations for long term sequestration.

Numerical modeling of the migration of the CO_2 plume is a prerequisite to effective CCS projects. It is used throughout the site screening, permitting, designing, operating, monitoring and closure processes (NETL, 2017). In a geological formation, the migration of the CO_2 is controlled by a complex interplay of viscous, capillary, and gravity forces. Once CO_2 is injected into the formation, it migrates away from the injection well while rising upward since CO_2 is lighter than the formation fluid. The injected CO_2 is subject to the risk of leakage if it encounters permeable faults or leaky well bores. Figure 1 shows a schematic of a CO_2 plume in a geological formation.

Current modeling approaches solve the relevant mass and energy balances using a set of spatially and temporally discretized nonlinear partial differential equations. However, this process is often computationally intractable due to the heterogeneity of geological formations, large spatial domains, and the long time frame of CO_2 sequestration (NAS, 2018).

The problem is confounded by the inherent uncertainty associated with the subsurface geology. Uncertainty analysis with stochastic simulations can be used to obtain probabilistic estimates of plume migration. However, stochastic simulations are limited by computational resources. Meanwhile, the model calibration process requires history-matching simulation models with monitoring data in an iterative fashion, which also requires huge computational resources (Kempka et al., 2010; Strandli et al., 2014; Zhang et al., 2014; Cowton
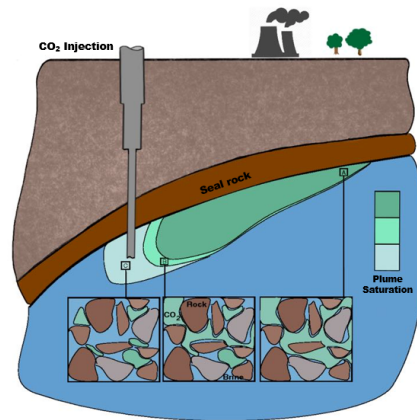
Proceedings of the 36th International Conference on Machine Learning, Long Beach, California, PMLR 97, 2019. Copyright 2019 by the author(s).

Figure 1. Schematic of CO_2 plume in geological formation (not to scale). Figure modified from Krevor et al. (2015).

et al., 2016). In practice, approximation approaches such as upscaling or reduced physics modeling have been heuristically developed to aid decision making (Nordbotten et al., 2012).

In recent years, we have seen some encouraging studies that apply neural networks to subsurface flow problems (Zhu & Zabaras, 2018; Mo et al., 2019). In both studies, the mapping from input properties (e.g. permeability) to output states (e.g. flow velocity, saturation, pressure) are treated as an image-to-image regression. Zhu and Zabaras (2018) proposed an encoder-decoder network to solve a 4,225-dimensional single-phase flow problem where the network predicts the flow velocity and pressure fields given a permeability map. Applying a similar encoder-decoder network, Mo et al. (2019) studied a 2,500-dimensional CO_2-water multiphse flow problem in the xy plane (no gravity). The injection time is added as an additional scalar input to the network and broadcast to a separate channel in the latent space to make predictions over time.

Extending on previous works, here we take an essential step by embedding spatial information in controlling parameters such as injection location and duration. We demonstrate that the network achieves high accuracy in 16,384-dimensional multiphase flow problems in the rz plane, where viscous, capillary, and gravity forces all play an important role. This

allows deep neural network approaches to be applied in more realistic CO$_2$ sequestration settings. This network also deals with discontinuous geological heterogeneities, which is crucial for many sequestration formations.

2. Data Description

Our dataset includes pairs of input permeability fields and output super-critical CO$_2$ saturation fields in a uniform grid of 128 x 128 with a grid size of 1 m. The proposed geological formation is located 1500 meters below ground surface in an isothermal reservoir. The permeability fields are randomly generated with laterally correlated heterogeneity to mimic the sedimentary formations that are typically used for sequestration. Correlation lengths for the permeability heterogeneity distributions range from a few meters to several hundred meters to represent the complex geology found in subsurface formations.

To incorporate the injection duration and location, we create a separate channel, where the injection well is treated as a CO$_2$ source term on the designated cell. Supercritical CO$_2$ is injected to the center of the cylindrical volume with a rate of 2.3 tons of CO$_2$ per day per meter of well perforation. An example of a training sample is included in Figure 2. This approach is scalable to more controlling parameters with spatial information (e.g. porosity, well bore pressure, initial saturation, etc.) which can be easily stacked as separate channels.
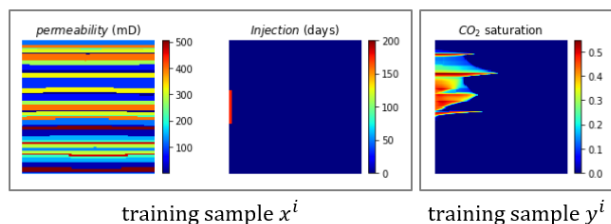

Figure 2. An example from the training set. The permeability, injection, and saturation fields all lie in a rz plane. The modeled volume is radially symmetrical and the injection well is located in the center of the cylindrical volume.

The CO$_2$ saturation field is calculated with the state-of-the-art full-physics numerical simulator ECLIPSE (Schlumberger, 2014). Each simulation takes around 15 minutes on an Intel Core i7-4790 CPU.

3. Neural Network Setup

The network is designed based on the U-Net architecture (Ronneberger et al., 2015) and the ResNet architecture (He et al., 2015). The task of the network is to predict the

x to y mapping from an input permeability field and an input injection field to the output CO$_2$ saturation field. The structure of the network is illustrated as Figure 3.
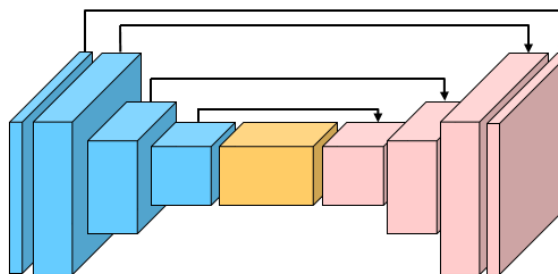

Figure 3. Schematic of the neural network. Blue represents en encoding unit, yellow represents a connecting unit, pink represents a decoding unit, and the black arrow represents a concatenating path.

The encoding path contains four encoding units (blue block) where each encoding unit contains a convolution layer, a batch normalization layer, and a Relu activation layer. By using 3x3 filters, the encoder extracts 128 channels of 16x16 feature map where each channel contains some latent representations of the input physical space.

A connecting unit (yellow block) contains five ResNet blocks to perform mapping from the input permeability latent representations to the output saturation latent representations.

The decoding units (pink block) each contain an up-pooling layer, a reflection padding layer, a convolution layer, a batch normalization layer, and an activation layer. The reflection padding layer is added to prevent artifacts around the edges of the output. Also, the concatenating channels merge the intermediate feature maps extracted from the encoding path with the corresponding decoding path and feed into the next decoding unit. The last decoding unit outputs the prediction of the CO$_2$ saturation map.

4. Result

4.1. Baseline

Baseline results of the CO$_2$ saturation map predicted by the proposed network is shown in Figure 4. The baseline model is trained with 40,000 training samples for 150 epochs. Each epoch takes around 2 minutes on an NVIDIA Tesla V100 GPU. At test time, each plume prediction takes around 0.0003 second, which is 6 orders of magnitude faster than ECLIPSE.

The results in Figure 4 demonstrate the network's ability to

make accurate predictions in highly stochastic formations (first row), channelized formations (second row), and layered formations (third row). The trained network estimates the saturation of CO_2 according to the injection duration and location while capturing the interplay of viscous, capillary, and gravity forces. The mean absolute error on the validation set is around 0.0015, which is considered negligible in the context of plume migration.
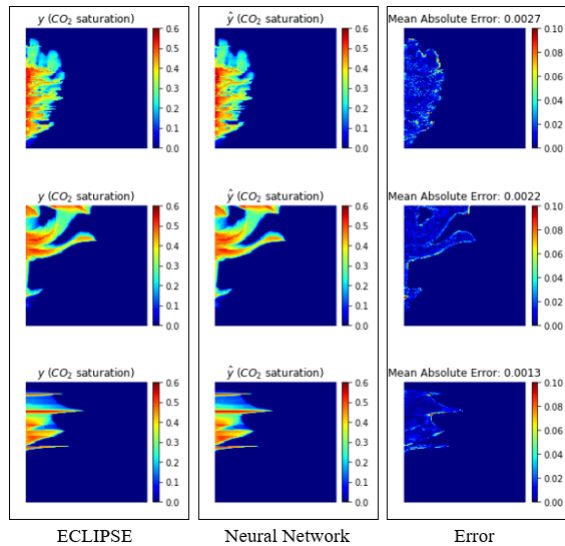

Figure 5. Mean absolute error on the validation set verse the number of training samples. The validation set contains 80 samples.

for the interpolate case and about 0.0170 for the extrapolate case. Figure 6 shows the results from the interpolation and the extrapolation cases.

Figure 4. Validation set results on the baseline model which is trained by 40,000 samples for 150 epochs.

4.2. Sensitivity to the number of training samples

Figure 5 shows the validation set errors trained by 40,000 to 40 samples. Surprisingly, the network that is trained by only 40 training samples still achieves low mean absolute error (0.015) on the validation set. Even with this small dataset, the neural network manages to learn an approximate shape of the plume.

4.3. Generalization

A key challenge in predicting plume migration with a neural network is whether the network can generalize outside of it's training data. We address this concern with the following sensitivity studies. The interpolation ability is demonstrated by using a training set that includes samples with 20, 60, 100, 140, and 180 days of injection, and a validation set that includes samples with 40, 80, 120, 160 and 200 days of injection. Similarly, the extrapolation ability is demonstrated by a training set with 20 to 120 days of injection, and a validation set with 120 to 200 days of injection.

The size of the training set is 20,000 for both cases. The mean absolute error on the validation set is about 0.0075
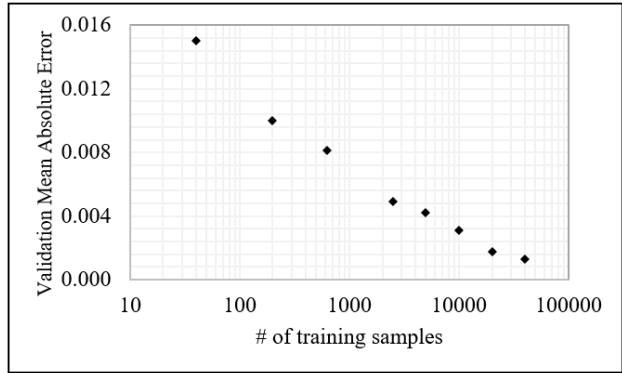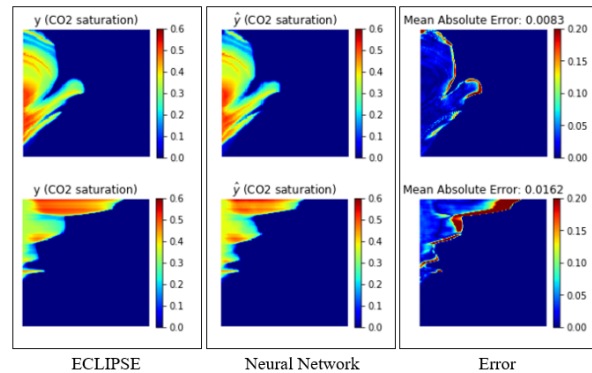
Figure 6. The first row demonstrates that the network can interpolate the plume with 160 days of injection form the training samples with 140 and 180 days of injection. The second row demonstrates that the network can extrapolate to 200 days of injection from the training samples with 20 to 120 days of injection.

5. Conclusion

In this paper, we provide an robust approach to conduct fast and accurate prediction of CO_2 plume by using deep neural networks. Our network can accurately predicts the CO_2 plume migration in high dimensional complex systems with highly heterogeneous subsurface geology. To show the potential of this approach, we also demonstrate the ability of this network to generalize outside of the training data. This approach can be easily adopted to history-matching and uncertainty analysis problems to support the scale-up of CCS deployment.

References

Cowton, L. R., Neufeld, J. A., White, N. J., Bickle, M. J., White, J. C., and Chadwick, R. A. An inverse method for estimating thickness and volume with time of a thin CO2-filled layer at the Sleipner Field, North Sea. *Journal of Geophysical Research: Solid Earth*, 121(7):5068–5085, 2016. ISSN 21699356. doi: 10.1002/2016JB012895.

He, K., Zhang, X., Ren, S., and Sun, J. Deep Residual Learning for Image Recognition. 2015. URL http://arxiv.org/abs/1512.03385.

IPCC. Climate Change 2014: Synthesis Report - Summary Chapter for Policymakers. *Contribution of Working Groups I, II and III to the Fifth Assessment Report of the Intergovernmental Panel on Climate Change [Core Writing Team, R.K. Pachauri and L.A. Meyer (eds.)]*, pp. 31, 2014. ISSN 1476-4687. doi: 10.1017/CBO9781107415324.

Kempka, T., Kühn, M., Class, H., Frykman, P., Kopp, A., Nielsen, C., and Probst, P. Modelling of CO2 arrival time at Ketzin Part I. *International Journal of Greenhouse Gas Control*, 4(6):1007–1015, 2010. ISSN 17505836. doi: 10.1016/j.ijggc.2010.07.005.

Krevor, S., Blunt, M. J., Benson, S. M., Pentland, C. H., Reynolds, C., Al-Menhali, A., and Niu, B. Capillary trapping for geologic carbon dioxide storage - From pore scale physics to field scale implications. *International Journal of Greenhouse Gas Control*, 40:221–237, 2015. ISSN 17505836. doi: 10.1016/j.ijggc.2015.04.006. URL http://dx.doi.org/10.1016/j.ijggc.2015.04.006.

Mo, S., Zhu, Y., Zabaras, N., Shi, X., and Wu, J. Deep Convolutional Encoder-Decoder Networks for Uncertainty Quantification of Dynamic Multiphase Flow in Heterogeneous Media. *Water Resources Research*, pp. 1–30, 2019. ISSN 19447973. doi: 10.1029/2018WR023528.

NAS. *Negative Emissions Technologies and Reliable Sequestration*. 2018. ISBN 9780309484527. doi: 10.17226/25259.

NETL. Best Practices: Risk Management and Simulation for Geologic Storage Projects. pp. 114, 2017. URL https://www.netl.doe.gov/sites/default/files/2018-10/BPM{_}RiskAnalysisSimulation.pdf.

Nordbotten, J. M., Flemisch, B., Gasda, S. E., Nilsen, H. M., Fan, Y., Pickup, G. E., Wiese, B., Celia, M. A., Dahle, H. K., Eigestad, G. T., and Pruess, K. Uncertainties in practical simulation of CO 2 storage. *International Journal of Greenhouse Gas Control*, 9:234–242, 2012. ISSN 17505836. doi: 10.1016/j.ijggc.2012.03.007. URL http://dx.doi.org/10.1016/j.ijggc.2012.03.007.

Ronneberger, O., Fischer, P., and Brox, T. U-net: Convolutional networks for biomedical image segmentation. *Lecture Notes in Computer Science (including subseries Lecture Notes in Artificial Intelligence and Lecture Notes in Bioinformatics)*, 9351:234–241, 2015. ISSN 16113349. doi: 10.1007/978-3-319-24574-4_28.

Schlumberger. ECLIPSE Reference Manual, 2014.

Strandli, C. W., Mehnert, E., and Benson, S. M. CO2 plume tracking and history matching using multilevel pressure monitoring at the Illinois basin - Decatur project. *Energy Procedia*, 63:4473–4484, 2014. ISSN 18766102. doi: 10.1016/j.egypro.2014.11.483. URL http://dx.doi.org/10.1016/j.egypro.2014.11.483.

Zhang, G., Lu, P., and Zhu, C. Model predictions via history matching of CO2 plume migration at the Sleipner Project, Norwegian North Sea. *Energy Procedia*, 63:3000–3011, 2014. ISSN 18766102. doi: 10.1016/j.egypro.2014.11.323. URL http://dx.doi.org/10.1016/j.egypro.2014.11.323.

Zhu, Y. and Zabaras, N. Bayesian deep convolutional encoderdecoder networks for surrogate modeling and uncertainty quantification. *Journal of Computational Physics*, 366:415–447, 2018. ISSN 10902716. doi: 10.1016/j.jcp.2018.04.018.